Scientific Research Publishing

Open Journal of Applied Sciences, 2024, 14, 2648-2660
https://www.scirp.org/journal/ojapps
ISSN Online: 2165-3925
ISSN Print: 2165-3917

Theoretical and Experimental Quantification of Solar Radiation through a Tracking System

Guy Christian Tubreoumya[1,2], Eloi Salmwendé Tiendrebeogo[1], Tchardja Combary[1], Téré Dabilgou[1,2], Jacques Nebié[1,2], Boubou Bagré[1], Alfa Oumar Dissa[1], Antoine Bere[1]

[1]Laboratoire de Physique et de Chimie de l'Environnement (LPCE), Université Joseph KI-ZERBO, Ouagadougou, Burkina Faso
[2]LAboratoire de Mathématiques et PhySique (LA.M.P.S), Université de Perpignan Via Domitia (UPVD), Perpignan, France
Email: guytubreoumya@yahoo.fr

How to cite this paper: Tubreoumya, G.C., Tiendrebeogo, E.S., Combary, T., Dabilgou, T., Nebié, J., Bagré, B., Dissa, A.O. and Bere, A. (2024) Theoretical and Experimental Quantification of Solar Radiation through a Tracking System. *Open Journal of Applied Sciences*, **14**, 2648-2660.
https://doi.org/10.4236/ojapps.2024.149174

Received: May 30, 2024
Accepted: September 24, 2024
Published: September 27, 2024

Abstract

This work deals with the estimation of solar radiation through a solar tracker aimed at evaluating the effect of solar tracking on the solar deposit in Burkina Faso. Using a two-axis solar tracking system, we experimentally measured solar radiation at our Joseph KI-ZERBO University site and compared it with that obtained by a numerical simulation run using Fortran programming software based on a mathematical model by Brichambaut. The results obtained from the mathematical and experimental studies show that, with a solar tracker, on a clear-sky day, solar irradiation is between 800 $W \cdot m^{-2}$ and 1000 $W \cdot m^{-2}$ between about 8 a.m. and 4 p.m., *i.e.* a duration of 8 hours of insolation. Analysis of the numerical and experimental results shows very good quantitative and qualitative agreement, with an average relative error of 18%.

Keywords

Tracking System, Solar Radiation, Dual Axis, Energy Efficiency

1. Introduction

A country's development depends to a large extent on its energy resources. However, the predominant sources of energy are fossil fuels, which are exhaustible and have a heavy negative impact on the environment through greenhouse gas emissions. Hence the need to turn to renewable energies, in particular solar energy, which is available in large quantities all over the world and inexhaustible on a human scale. In Burkina Faso, in particular, geological excavations make no mention of the existence of huge fossil deposits underground [1]. Nevertheless, it is a very sunny country, with an estimated solar potential of 5.5 $Kwh \cdot m^{-2} \cdot Jr^{-1}$ and an estimated 8.3 hours of insolation per day [2]. However, the amount of solar

radiation is not the same throughout the day, or throughout the year and in different geographical locations, due to the apparent movement of its source.

This is why solar tracking systems have been developed to constantly direct their collecting surface towards the sun, perpendicular to the sun's rays and following the sun as it moves. This optimizes their performance [3].

Several authors have already tackled the study of solar tracking systems. Some have approached it through modeling studies (Grazyna *et al.* (2015), Amelia *et al.* (2020), Maiga, A. (2021)) and others have conducted experimental studies (Dib *et al.*, (2019), Benbouza, (2008), Jeong *et al.* (2017)) [4]-[9]. In Burkina Faso, solar power systems are fixed with a tilt angle equal to the latitude of the site. This is the case for the Zagoutouli (33 MWp), Ziga (1.1 MWp) and Nagréongo (30 MWp) solar power plants [10]. The country has practically no system equipped with solar tracking. It is in this context that this article aims to study solar radiation through a solar tracking system. The general aim of this study is to quantify solar radiation through a solar tracking system and to assess the effect of tracking systems on the country's solar potential. More specifically, it will involve experimentally measuring solar radiation at our site using a sun-tracking device, and modeling solar radiation through a tracking system in order to validate the proposed numerical model.

2. Modeling Solar Radiation through a Tracking System

The absence of large-scale weather stations has led to the use of mathematical models to obtain solar radiation data for a given geographical location. Several models have been established for this purpose, the best known and most widely used being the Brichambaut and Liu-Jordan models [11] [12]. Benkaciali and Gairaa, in 2011, based on a comparative analysis of the Liu-Jordan and Brichambaut models, obtained results that were considered satisfactory for most energy analyses [13]. The Liu-Jordan model does not use the atmospheric haze factor, compared with the Brichambaut model. Their study shows that the Brichambaut model gives better results than the Lui-Jordan model [14] [15]. The theoretical Brichambaut model has been chosen for the simulation of global solar irradiation at our Joseph KI-ZERBO University (UJKZ) site. This model was chosen because it is one of the best in the scientific literature for simulating solar irradiance at a given geographical location. It also takes atmospheric turbulence into account, and is the most commonly used model after Liu Jordan's model.

2.1. Global Radiation

In Brichambaut's theoretical model, the global radiation (G) incident on a flat surface equipped with a solar tracking system is calculated as the sum of direct radiation, diffuse radiation from the sky and diffuse radiation from the ground. The radiation equation is given by expression (1) [5].

$$G = S + \text{Dciel} + \text{Dsol} \quad (1)$$

2.2. Direct Irradiance

The direct illuminance incident on a clear sky on the collector surface with solar tracking of angle of inclination β and angle γ is given by the relationship:

$$S = \left(I_0 - 31 \times T_L\right) \times \exp\left(\frac{-ma \times T_L}{0.9 \times ma + 9.4}\right) \tag{2}$$

where T_L is the Linke disorder expressed as a function of the Angstrom coefficient and the condensable water head ω whose equation is given by:

$$T_L = 2.5 + 16 \times \beta_A + 0.5 \ln\left(\Omega\right) \tag{3}$$

The values of the coefficients and ω are given in Table 1.

Table 1. Angstrom constant and condensable water height according to the nature of the sky [4].

Sky nature	β_A	Ω
Pure	0.05	1
Medium	0.1	2
Gradient	0.2	5

$$ma = \frac{1}{\sin\left(h\right) + 9.40 * 10^{-4} \times \left(\sin\left(h\right) + 0.0678\right)^{-1.253}} \tag{4}$$

The solar elevation angle h is given by:

$$\sin\left(h\right) = \sin\left(\varphi\right) \times \sin\left(\delta\right) + \cos\left(\varphi\right) \times \cos\left(\delta\right) \times \cos\left(\omega\right) \tag{5}$$

2.3. Diffuse Irradiance

Diffuse irradiance is the sum of diffuse sky D_{ciel} and diffuse ground D_{sol}. Diffuse sky irradiance is given by expression (6) [5]:

$$D_{ciel} = \frac{87 \times \left(\sin\left(h\right)\right)^{0.4}}{1 + \sin\left(h\right)} \times \left(1.5 + 0.5 \times \sin\left(h\right)\right) \tag{6}$$

where h is the angular height of the sun.

Diffuse ground irradiance is given by relationship (7) [5]:

$$D_{sol} = 0.5 \times \rho \times G_h \times \left(1 - \sin\left(h\right)\right) \tag{7}$$

where ρ is the albedo of the site under consideration and G_h is the global irradiance on a horizontal flat-plate collector. Fortran software was then used to program the equations governing the global solar irradiance of the mathematical model on our site.

3. Experimental Study of Solar Radiation through a Tracking System

3.1. Presentation of the Experimental Set-Up

Our TRACSOL solar tracker is a mechanical system with two axes of rotation and

two (02) 30W-18V-1.6A monocrystalline PV modules providing the system with energy autonomy for motor operation. The motor housing, as shown in Figure 1 and Figure 2, has an azimuthal (vertical) axis and a zenithal (horizontal) axis (chain + sprocket motor) with limit switches, enabling the TRACSOL to rotate around itself. This enables the TRACSOL to follow the sun's path in real time. Global solar radiation measurements at our site were carried out using a Spektron 320 solarimeter, mounted on a two-axis solar tracking system (TRACSOL). The error committed by the solarimeter during a given measurement is estimated at 5%. Using a METEON-type data logger, the measured radiation data are stored and subsequently processed to obtain solar radiation curves as a function of time. The data logger reading error is estimated at 1%.

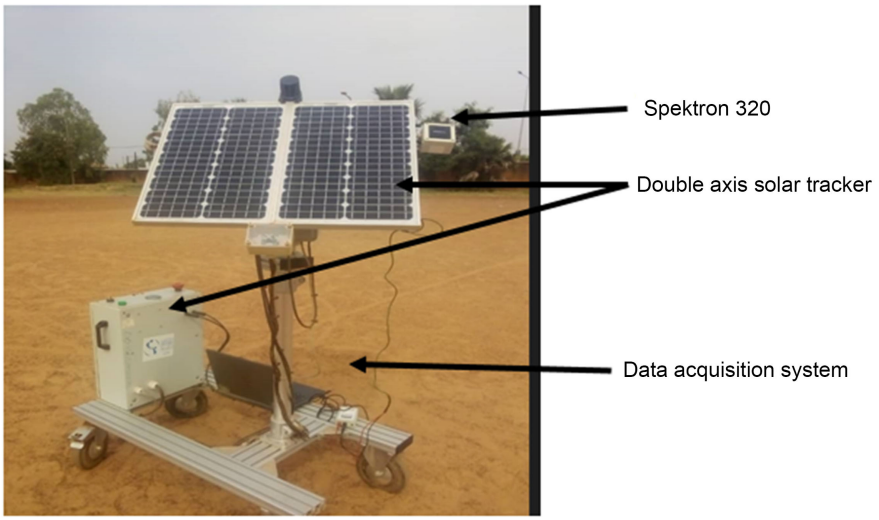

Figure 1. Experimental set-up.

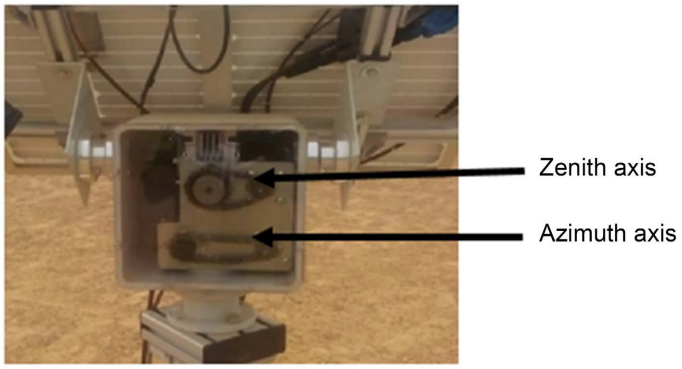

Figure 2. Motor housing.

3.2. Experimental Protocol

The measurement periods concerned the typical days of a few months in the year 2023. A typical day, for a given month, represents the average day when solar radiation is imposed compared to other days of the same month.

Table 2 shows the typical days from Liu and Jordan's analysis. We will carry

out our modelling and experimentation taking these typical days of the month into account.

Table 2. Typical days in the analysis by Liu *et al.* [16].

Month	January	February	March	April	May	June	July	August	September	October	November	December
number of the day	**1**	**2**	**3**	**4**	**5**	**6**	**7**	**8**	**9**	**10**	**11**	**12**
month number	**17**	**16**	**16**	**15**	**15**	**11**	**17**	**16**	**15**	**15**	**14**	**10**
year numbers	**17**	**47**	**75**	**105**	**135**	**162**	**198**	**228**	**258**	**288**	**318**	**344**

The various measurements began in January 2023 and will continue until May 2023. The duration of the experiment is approximately 11 hours. It starts at around 07:00 and finishes at around 18:00. Firstly, at the start of each experiment, the experimental rig is set up, with the solar radiation measurement system (Solar meter) positioned horizontally in relation to the solar panels fitted with the two-axis tracking system, keeping it continuously perpendicular to the sun's rays, and then the solar tracking system is switched on. Next, connect the solar meter to the "Data logger" data acquisition system by switching on the data logger. Finally, using a USB cable, connect the data logger to a computer running Meteon software, and start recording. Programming consists in opening the Meteon software installed on the computer's Windows operating system; first, select the pyranometer and the appropriate sensitivity (in our case, SP Lite 2 with 100 mV sensitivity); second, select the time step (for our measurements, a 5-minute time step was chosen) and the start-up or recording begins automatically. Verification is carried out by directly reading the various solar radiation values on the data acquisition and/or by visualizing the evolution of the solar irradiation curve using a computer connected to the data acquisition. After each measurement at the end of the day, the data acquisition is downloaded to a computer via a USB cable, where the data is saved.

4. Results and Discussion

4.1. Theoretical Results

The curves in **Figure 3** and **Figure 4** represent the hourly evolution of global solar irradiance incident on a flat surface fitted with a sun tracker according to Brichambaut's theoretical model for typical days in January, February, March and April.

Global solar radiation, according to Brichambaut's semi-empirical model has the same variations for the different typical days of the four months considered. In fact, all the curves have the same bell-shaped appearance, peaking at solar noon for each of them. The radiation value at the top is around 1000 $W \cdot m^{-2}$. Our results confirm the work of Draou *et al.* (2008), who studied a control system for a sun tracker. They used the Brichambaut model to model the global radiation incident

on a sensor fitted with a sun-tracking system, and obtained theoretical bell-shaped curves with a peak value of around 1000 $W \cdot m^{-2}$ [4].

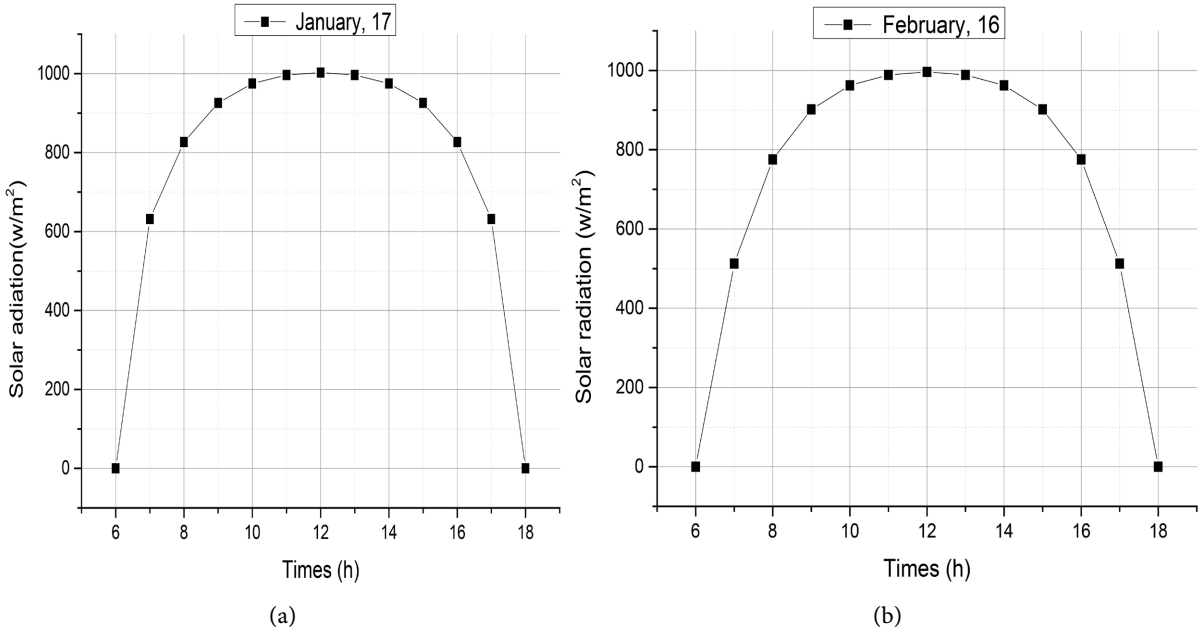

(a) (b)

Figure 3. Hourly evolution of theoretical global solar radiation for the days of January 17 and February 16.

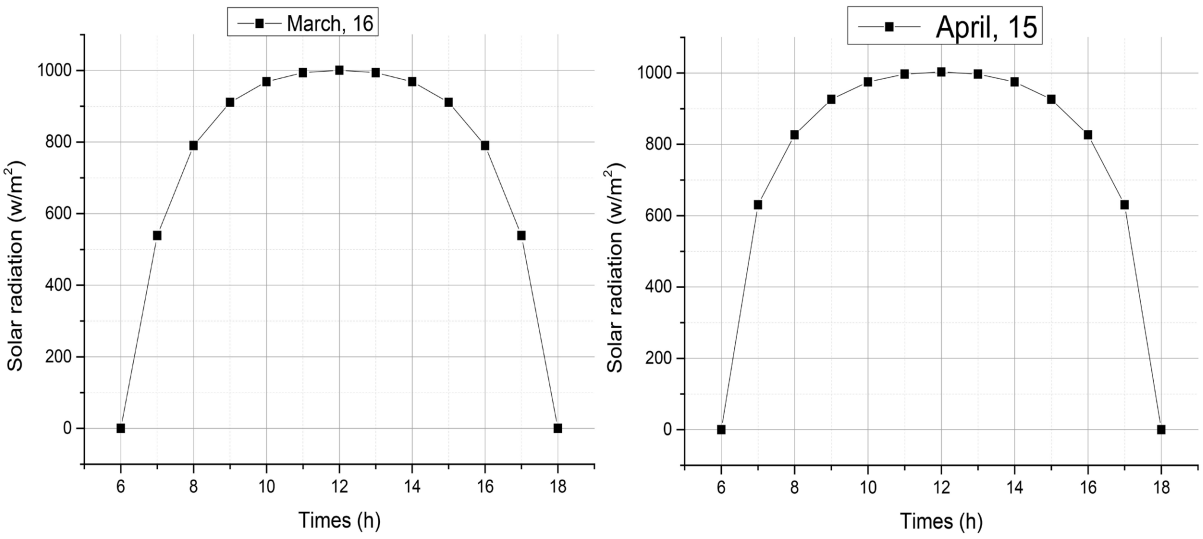

(a) (b)

Figure 4. Hourly evolution of theoretical global solar radiation for the days of March 16 and April 15.

We can also see that the solar radiation curves for typical days in each month fall between 7 am and 10 am. They then remain more or less constant from 10 am to 2 pm, when they practically reach their maximum values; before decreasing slightly from 2 pm to 4 pm, and finally decreasing significantly from 4 pm to 6 pm, until they reach zero.

Furthermore, an analysis of the curves obtained shows that the global solar

radiation values achieved from 08:00 to 16:00 are between 800 $W \cdot m^{-2}$ and 1000 $W \cdot m^{-2}$, which corresponds to a good range of sunshine throughout the country's insolation period, estimated at around 8.3 $h \cdot dr^{-1}$.

4.2. Experimental Results

Figure 5 and Figure 6 below show the experimental curves obtained on the experimental days of January 17, February 16, March 16 and April 15, 2023.

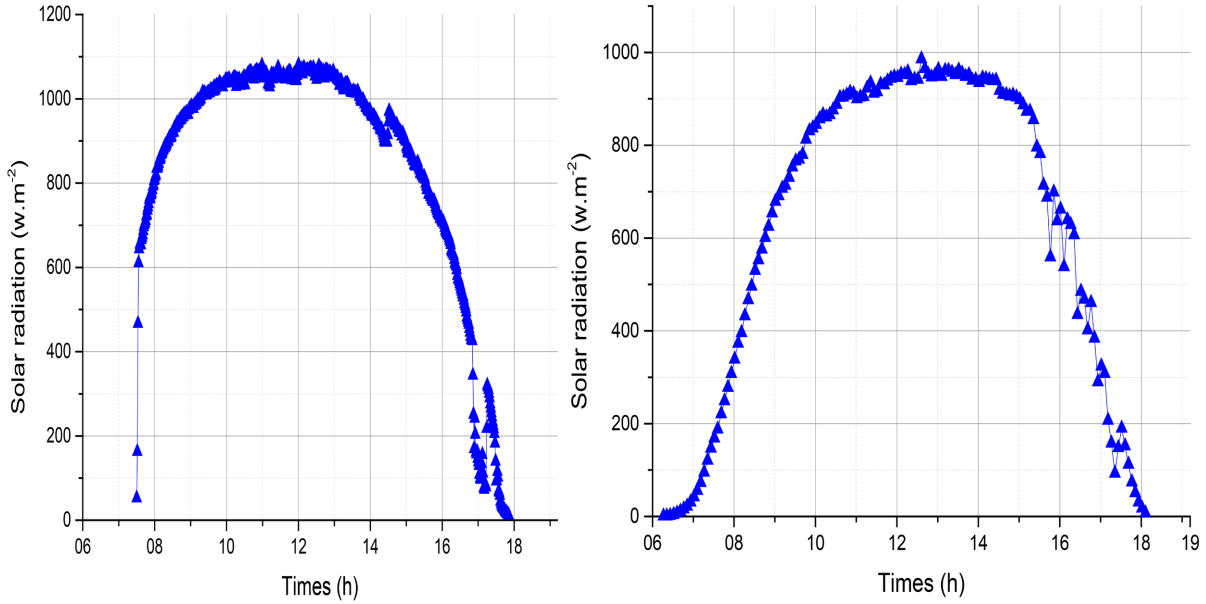

Figure 5. Hourly variation in global solar radiation measured on January 17 (a) and February 16 (b) 2023.

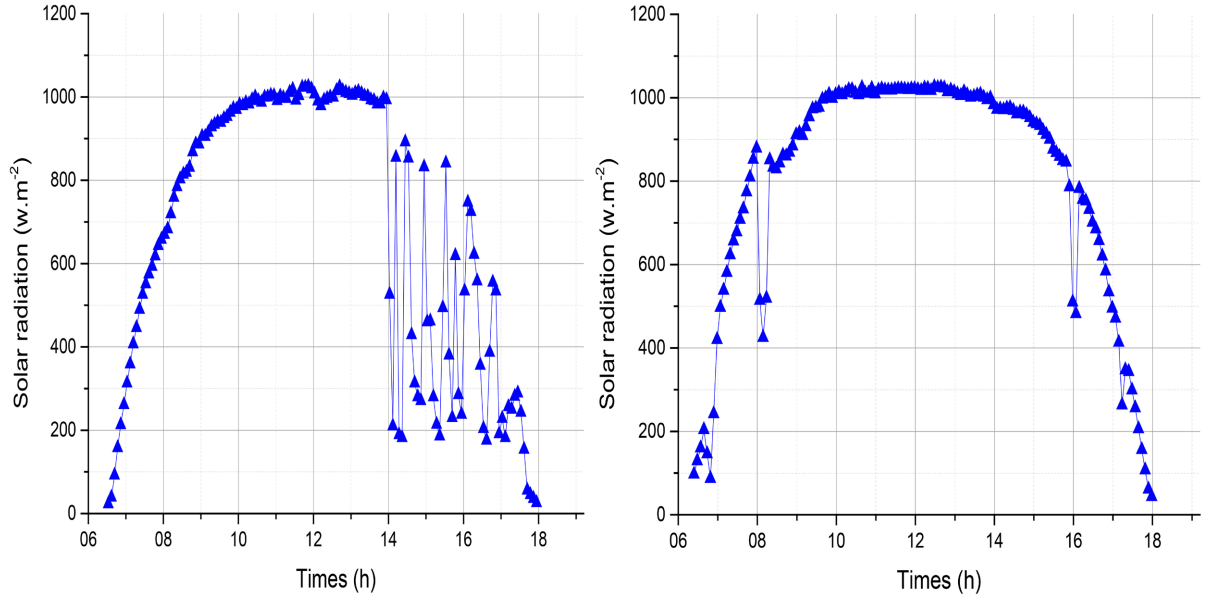

Figure 6. Hourly variation in global solar radiation measured on March 16 (a) and April 15 (b) 2023.

All the experimental curves show that solar radiation varies throughout the day. Values at sunrise and sunset are low, while those at solar noon are at their highest. The peak of the curves reached at solar noon is around 1000 $W \cdot m^{-2}$. All curves have the same bell-shaped appearance.

Analysis of the experimental global radiation curve for a typical day in January shows that over the time interval from 8 am to 3:30 pm, radiation values range from 800 $W \cdot m^{-2}$ to over 1000 $W \cdot m^{-2}$. Between 14:00 and 14:30 min, there is a slight fluctuation, which certainly explains the radiation value below 800 $W \cdot m^{-2}$ before 16:00.

In Figure 5(b), global radiation values between 800 $W \cdot m^{-2}$ and 1000 $W \cdot m^{-2}$ are observed over the time interval from 9 h 45 min to 15 h 30 min, but there is also a slight disturbance from sunrise until almost 10 h, and this disturbance, compared to that of the morning, becomes significant from 15 h until sunset.

For the typical day in March, despite the strong fluctuation, global radiation values between 800 $W \cdot m^{-2}$ and 1000 $W \cdot m^{-2}$ can be observed over the 8 a.m. to 4 p.m. time interval if the curve is continued in the absence of the disturbance.

Analysis of the global radiation curve for a typical day in April clearly shows that over the time interval from 8 a.m. to 4 p.m., radiation values range from 800 $W \cdot m^{-2}$ to 1000 $W \cdot m^{-2}$.

In general, on all typical days of the different months, maximum incident sunshine is observed over the insolation period. In the middle of the day, global radiation reaches values of 1000 $W \cdot m^{-2}$.

Analysis of these figures reveals that solar radiation curves increase from 7 am to 10 am. They remain more or less constant from 10 a.m. to 2 p.m., when they practically reach their maximum values; then they decrease slightly from 2 p.m. to 4 p.m., before decreasing significantly from 4 p.m. to 6 p.m., when the curves cancel each other out. The same observations were made by Nomao *et al.* (2022) in a study estimating direct solar radiation, obtaining curves similar to ours; the only difference is that they obtained a constant curve from 10 a.m. to 4 p.m., whereas in our case, the curve is constant from 10 a.m. to 2 p.m. and decreases slightly until 4 p.m. [15].

We also observe fluctuations of varying magnitude on certain curves, but especially on the curve obtained for the day of 16/03/2023, where the fluctuations are more intense, covering the whole afternoon. These fluctuations can be explained by the passage of certain obstacles such as clouds, aerosols or dust mists. As Kombassere, 2022 and many other studies have shown, these obstacles are the main causes of solar radiation attenuation at ground level, and consequently influence solar panel efficiency [17]. Similarly, a study by Koussa *et al.* (2007) shows that on clear-sky days, the amount of solar radiation on the collector surface is significantly higher than on horizontal and inclined planes, increasing panel output by up to 30% at 40% [18].

4.3. Validation of the Numerical Model

Figure 7 and Figure 8 below show a comparison of the theoretical results of the

Brichambaut model with the experimental results of global solar radiation for typical days in January, February, March and April of the year 2023.

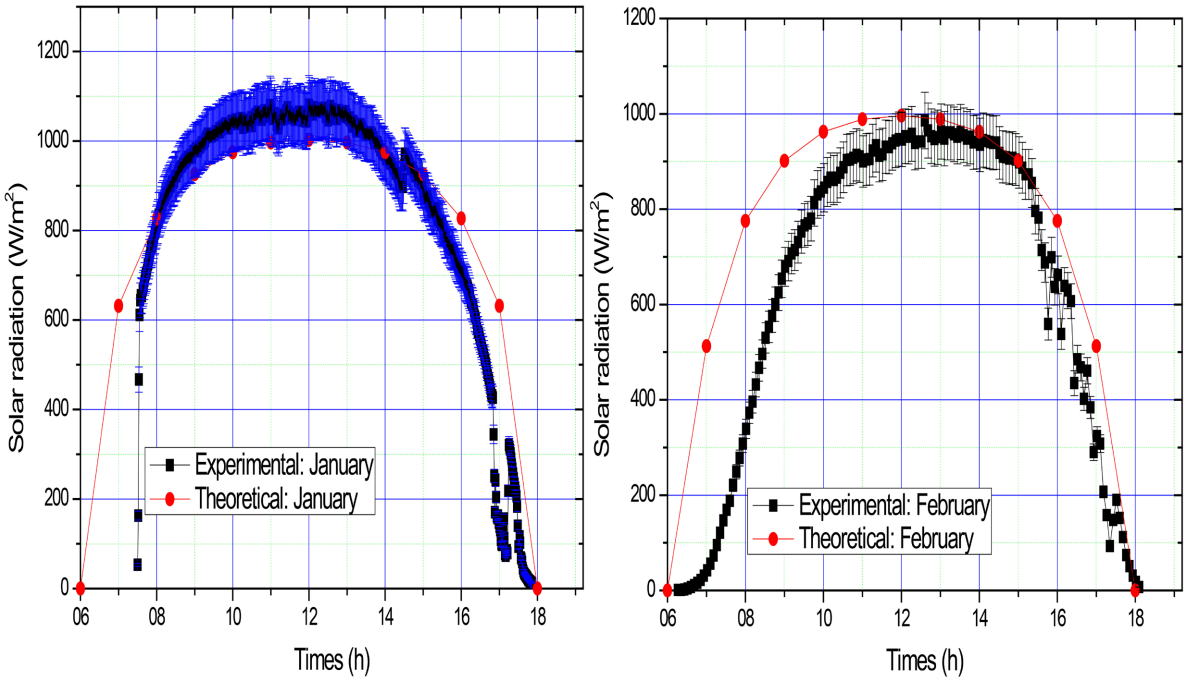

Figure 7. Hourly comparison of theoretical and experimental global solar radiation on January 17 and February 16.

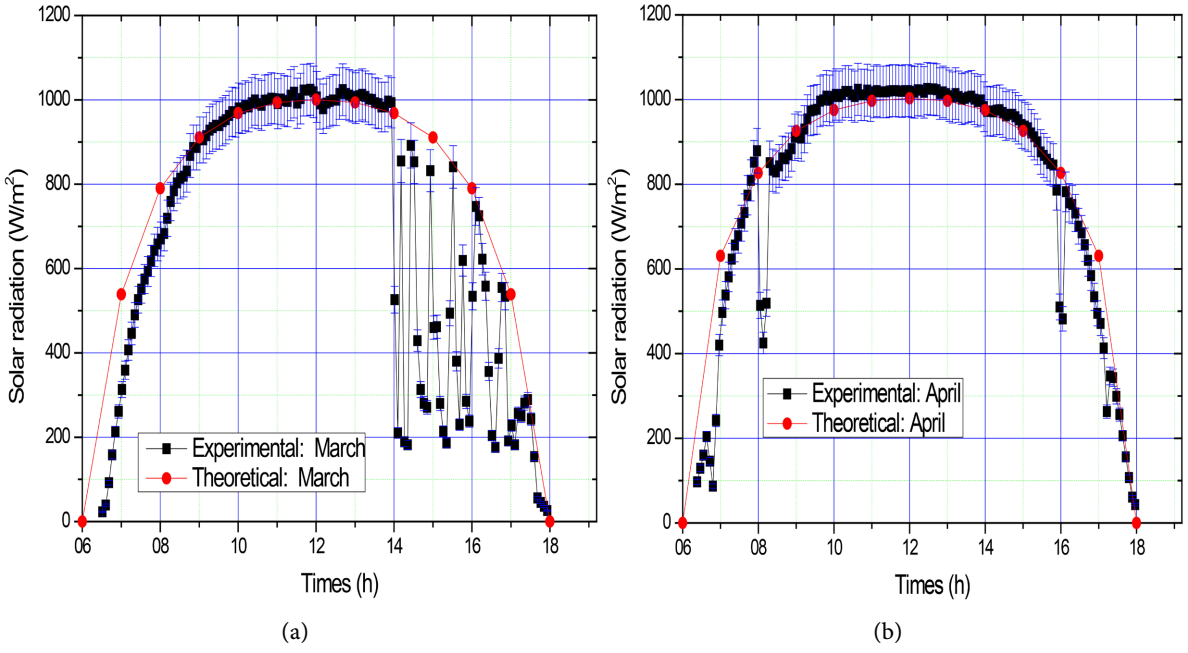

Figure 8. Hourly comparison of theoretical and experimental global solar radiation on March 16 and April 15.

All the experimental and theoretical curves in **Figure 7** and **Figure 8** show the same bell-shaped curves, indicating that solar radiation varies throughout the day.

Analysis of the two curves in Figure 7 for the January day shows that the theoretical model overestimates the experimental measurement at sunrise and in the afternoon from 4 pm. There is a good approximation between the theoretical curve and that of the solar radiation measured at the site from 08:00 to 15:30 on the January day.

The daytime curves for the month of February show that the Brichambaut model overestimates measured radiation from sunrise to 10:30 am, as well as from 4 pm onwards. The difference between the theoretical and experimental curves is significant in the morning, but only slight in the afternoon at 4 pm. The two curves match from solar noon until around 14 h 45 min. For the typical day in March, the analysis shows a good approximation between the theoretical and experimental curves, from sunrise until 1 pm, when the theoretical model overestimates the measured solar radiation due to the strong climatic disturbance. There is a very slight discrepancy between the two curves just at sunrise. In the absence of fluctuation, the theoretical and experimental curves match from 08:00 to sunset. Analysis of the curves for the month of April shows a good approximation between the two curves from sunrise to sunset. However, there was a slight overestimation of the theoretical model just at sunrise.

The discrepancies between the theoretical and experimental curves are certainly due to the fluctuations observed on the experimental curves. In fact, these fluctuations, due to climatic disturbances, appear to attenuate solar radiation on the ground. The clear-sky condition adopted for the numerical model also leads to high theoretical solar radiation values, compared with experimental values where the sky is often disturbed by cloudy passages, dust and aerosols. Finally, the problem of calibrating measurement systems can also contribute to the discrepancies observed between theoretical and experimental curves. This leads to an increase in the mean relative error of Brichambaut's mathematical model. Overall, Brichambaut's estimation model on a plane fitted with a solar tracker gives a satisfactory agreement with the values measured on our study site.

Similar studies have been carried out by O. B. Boudi *et al.* (2007) who modelled and validated the solar potential of the Nouakchott and Dakar sites. Their study shows that for clear-sky days, the curves show the same pattern, with deviations observed during certain months reaching a maximum relative value of 18.75% (December 1) at the Nouakchott site, with significant attenuation observed between 12 and 5 pm at the Nouakchott site, which would be due to cloudy disturbances [19].

5. Conclusions

In this article, we measured global solar radiation at our study site using an experimental device, a two-axis sun-tracking system. The measured radiation values were compared with those of the Brichambaut model.

With a solar tracker on a clear-sky day, solar irradiation is between 800 $W \cdot m^{-2}$ and 1000 $W \cdot m^{-2}$ during the time interval from 08:00 to 16:00. This means that,

over the duration of the country's insolation, a solar collector equipped with a sun tracker will always receive maximum radiation at its surface.

Analysis of our numerical and experimental results also shows very good quantitative and qualitative agreement. In Burkina Faso, for example, where there is a lot of sunshine, solar trackers will help to solve the energy problem.

Conflicts of Interest

The authors declare no conflicts of interest regarding the publication of this paper.

References

[1] Ouédraogo, S. (2023) Production de la vapeur d'eau par le rayonnement solaire en circuit court à l'aide d'un concentrateur cylindro-parabolique composé (CPC). Thèse de doctorat en Physique énergétique Université Joseph Ki-Zerbo, 225 p.

[2] Azoumah Y, *et al.* (2010) Siting Guidelines for Concentrating Solar Power Plants in the Sahel: Case Study of Burkina Faso. *Solar Energy*, **84**, 1545-1553. https://doi.org/10.1016/j.solener.2010.05.019

[3] Nadhir, B. and Abdelkarim, H. (2022) Etude et simulation d'un système de poursuite solaire. PhD Thesis, University of M'sila, 90 p.

[4] Draou, M.D. and Droui, B. (2008) Etude, conception et expérimentation d'un système de contrôle pour système suiveur de soleil. *Revue des Energies Renouvelables*, **11**, 229-238.

[5] Benbouza, N. (2008) Etude du rayonnement solaire dans la région de Batna. Mémoire de Magister en Electrotechnique, Université de Batna, 98 p.

[6] Frydrychowicz-Jastrzębska, G. and Bugała, A. (2015) Modeling the Distribution of Solar Radiation on a Two-Axis Tracking Plane for Photovoltaic Conversion. *Energies*, **8**, 1025-1041. https://doi.org/10.3390/en8021025

[7] Amelia, R., Irwan, Y.M., Safwati, I., Leow, W.Z., Mat, M.H. and Rahim, M.S.A. (2020) Technologies of Solar Tracking Systems: A Review. *IOP Conference Series*: *Materials Science and Engineering*, **767**, Article ID: 012052. https://doi.org/10.1088/1757-899X/767/1/012052

[8] Dib, K. and Chenni, R. (2019) Contribution à la réalisation d'un suiveur solaire et d'une commande MPPT hybride dédiés aux applications photovoltaïques. Thesis, Université Frères Mentouri-Constantine 1. http://depot.umc.edu.dz/handle/123456789/5769

[9] Jeong, K., Hong, T., Koo, C., Oh, J., Lee, M. and Kim, J. (2017) A Prototype Design and Development of the Smart Photovoltaic System Blind Considering the Photovoltaic Panel, Tracking System, and Monitoring System. *Applied Sciences*, **7**, Article No. 1077. https://doi.org/10.3390/app7101077

[10] Maiga, A. (2021) Theoretical Comparative Energy Efficiency Analysis of Dual Axis Solar Tracking Systems. *Energy and Power Engineering*, **13**, 448-482. https://doi.org/10.4236/epe.2021.1312031

[11] Bignan-Kagomna, B., Ouedraogo, I., Koumbem, D.W.N. and Tchabode, G. (2022) Numerical Modelling of a Parabolic Trough Concentrator for the Design of a Thermodynamic Solar Power Plant. *American Journal of Energy Engineering*, **10**, 85-91. https://doi.org/10.11648/j.ajee.20221004.11

[12] Tahar, B.M. (2012) Etude théorique et expérimentale des paramètres de fonctionnement d'un capteur solaire plan. Magister en: Génie méca-nique, Université Mohamed Khider-Biskra, 119 p.

[13] Housseyn, B. and Rachid, K. (2017) Estimation de rayonnement solaire par deux méthodes. Master Génie Mécanique.

[14] Moummi, A., Hamani, N., Moummi, N. and Mokhtari, Z. (2006) Estimation du rayonnement solaire par deux approches semi empiriques dans le site de Biskra. 8*ème Séminaire International sur la Physique Energétique*, Centre Universitaire de Béchar-Algérie, 6.

[15] Nomao, H.S.D., Maikano, H.B., Sido, M.P. and Boukar, M. (2022) Study of Four (4) Semi-Empirical Models for Estimating Direct Radiation from the Sun and Modeling for Application to the Solar Thermodynamic System. *European Journal of Applied Sciences*, **10**, 765-782. https://doi.org/10.14738/aivp.104.12950

[16] Ouedraogo, E., Coulibaly, O. and Ouedraogo, A. (2012) Elaboration d'une année météorologique type de la ville de Ouagadougou pour l'étude des performances énergétiques des bâtiments. *Revue des Energies Renouvelables*, **15**, 77-90.

[17] Kombassere, J.G. (2022) Etude théorique et expérimentale de l'effet des pas-sages nuageux sur les performances électriques des installations photovoltaïques. Master recherche en sciences et technologies, Université Joseph KI-ZERBO, 57 p.

[18] Koussa, M., Malek, A. and Haddadi, M. (2007) Apport énergétique de la poursuite solaire sur deux axes par rapport aux systèmes fixes. Application aux capteurs plans. *Revue des Energies Renouvelables*, **10**, 515-537.

[19] Ould Bilal, B., Sambou, V., Kébé, C.M.F., Ndongo, M. and Ndiaye, P.A. (2007) Etude et modélisation du potentiel solaire du site de Douakchott et de Dakar. *Journal des Sciences*, **7**, 57.

Nomenclature

D_{ciel}	: Incident diffuse radiation from the sky	($W \cdot m^{-2}$)
D_{sol}	: Incident diffuse radiation from the ground	($W \cdot m^{-2}$)
G	: Incident global radiation on sun tracking plane	($W \cdot m^{-2}$)
G_h	: Global radiation on the horizontal plane	($W \cdot m^{-2}$)
h	: Sun height	(˚)
I_0	: Solar constant	($W \cdot m^{-2}$)
S	: Direct radiation on the plane with sun tracker	($W \cdot m^{-2}$)
T_L	: Linke disturbance factor	…
Z	: Site altitude	(m)
ρ	: Soil albedo	…
φ	: Latitude of location	(˚)
β	: Plan inclinaison to the horizontal	(˚)
δ	: Solar declinaison	(˚)
ω	: Clockwise angle	(˚)
γ_s	:Solar azimuth	(˚)
γ	: Collector azimuth	(˚)
θ_i	: Incident angle	(˚)